










Proceedings Article

# Experimental parameter calibration of the scanner model for model-based MPI

Florian Thieben <sup>a,b</sup> · Hannes Albers <sup>c</sup> · Fabian Mohn <sup>a,b</sup> · Fynn Foerger <sup>a,b</sup> ·  
Marija Boberg <sup>a,b</sup> · Konrad Scheffler <sup>a,b</sup> · Martin Möddel <sup>a,b</sup> · Tobias Kluth <sup>c</sup> ·  
Tobias Knopp <sup>a,b</sup>

<sup>a</sup>Section for Biomedical Imaging, University Medical Center Hamburg-Eppendorf, Hamburg, Germany

<sup>b</sup>Institute for Biomedical Imaging, Hamburg University of Technology, Hamburg, Germany

<sup>c</sup>Center for Industrial Mathematics, University of Bremen, Bremen, Germany

\*Corresponding author, email: [florian.thieben@tuhh.de](mailto:florian.thieben@tuhh.de)

© 2024 Thieben *et al.*; licensee Infinite Science Publishing GmbH

This is an Open Access article distributed under the terms of the Creative Commons Attribution License (<http://creativecommons.org/licenses/by/4.0>), which permits unrestricted use, distribution, and reproduction in any medium, provided the original work is properly cited.

## Abstract

Model-based reconstruction is still one of the key challenges in magnetic particle imaging (MPI) when using multi-dimensional Lissajous-type excitation. Besides an appropriate particle model, the model of the MPI system for signal generation and reception has a major impact on the modeled system matrix. We outline the influence of the MPI scanner parameters on the system matrix pattern and review methods to calibrate each parameter.

## 1. Introduction

Image reconstruction in magnetic particle imaging (MPI) often utilizes a system matrix that contains the spatial and scanner specific signal response of a small defined magnetic nanoparticle (MNP) sample, which is measured on a grid inside the field-of-view (FOV). This spatial calibration measurement is very time consuming and needs to be repeated for each new MNP type and field excitation type. An approach to bypass these time consuming calibration measurements is to simulate the system matrix with a suitable model [1, 2]. This model-based approach to simulate MNPs magnetization response goes back to the early years of MPI [3] and its accuracy is influenced by two underlying aspects, the *particle magnetization model* and the *MPI scanner model*. So far, modeling approaches have been developed under the assumption of ideal scanner setups with a strong focus on the magnetization model. Inside an applied magnetic field, the Langevin theory of paramagnetism for isotropic/anisotropic MNPs or Brownian/Néel magneti-

zation dynamics results in adequate simulations of the *particle magnetization model* by, for example, using a Fokker-Planck approach or more efficient Fourier neural operator approximations to provide the desired magnetization model [4, 5].

However, the modeled system matrix is strongly influenced by the MPI scanner in use, including its characteristic excitation signal and specific receive path [6, 7]. In contrast to the model-based approach with an idealized scanner model, the measured system matrix inherently contains all distortions caused by non-ideal spatiotemporal profiles of

- all magnetic fields and
- all receive path components.

In MPI, the magnetic field can be considered as a superposition of a static selection field, a static or slowly varying focus field, and a dynamic excitation/drive field. The receive path describes how the spatial receive coil sensitivity, analog filter, and low-noise amplifier distort the induced magnetization response. Only a precise *particle magnetization model* together with a well calibrated

*MPI scanner model* can generate a modeled system matrix that matches a measured one in amplitude and phase for a wide frequency bandwidth. Conversely, the parameters of the *particle magnetization model* can only be meaningful interpreted once the *MPI scanner model* has been calibrated.

In this work, we focus on the experimental calibration of the *MPI scanner model* that is performed independent of the *particle magnetization model*. Moreover, we investigate the influence of each model parameter on the accuracy of the resulting modeled system matrix. We review methods to identify these parameters in form of a magnetic field characterization and in form of the receive path calibration. We present a method for a more precise characterization of the drive-field sequence. Further, we present a method to identify a delay due to digital signal processing.

## II. Methods and materials

The setting of a general MPI imaging experiment reads as follows: Let  $\Omega \subset \mathbb{R}^3$  be the FOV containing MNPs. A voltage induced by the MNPs in a receive coil with sensitivity profile  $p : \mathbb{R}^3 \rightarrow \mathbb{R}^3$  in  $\text{m}^{-1}$  after passing through the receive path  $a : \mathbb{R} \rightarrow \mathbb{R}$  in Hz is approximately given by

$$\tilde{u}_M(t) = - \left( a * \mu_0 \int_{\Omega} c(r) p(r)^T \frac{\partial}{\partial t} \bar{m}(H(r, \cdot)) \, dr \right) (t) \quad (1)$$

in V, where  $\mu_0$  is the vacuum permeability in  $\text{kg m A}^{-2} \text{s}^{-2}$ ,  $c : \Omega \rightarrow \mathbb{R}_0^+$  in  $\text{mol L}^{-1}$  is the concentration of the magnetic nanoparticles, and  $\bar{m} : \mathbb{R}^3 \times [0, T] \rightarrow \mathbb{R}^3$  in  $10^{-3} \text{Am}^2 \text{mol}^{-1}$  is the molar mean magnetic moment.  $\bar{m}$  is given by a *particle magnetization model* and it depends on the applied magnetic field  $H : \mathbb{R}^3 \times [0, T] \rightarrow \mathbb{R}^3$  in  $\text{T} \mu_0^{-1}$ . The MPI scanner parameters  $a$ ,  $p$ , and  $H$  are attributes of the *MPI scanner model*. Considering an authentic *MPI scanner model*, the latter attributes may contain imperfections in form of magnetic field distortions and receive signal distortions and thus need to be determined precisely.

### II.I. Magnetic field distortions

Distortions of the magnetic field can occur in two ways, spatially and temporally. MPI coil assemblies exhibit magnetic field imperfections that increase in proximity of the coil. However, with the magnetic field as an input parameter of the *particle magnetization model*, the amplitude, homogeneity, and signal phase influence the generated system matrix. In Figure 1 a), the distortion of the Lissajous trajectory due to inhomogeneous magnetic fields is shown. Underlying, two 2D complex color coded system-matrix patterns regarding a homogeneous and an inhomogeneous magnetic field are shown. Boberg et al. showed that both fields and

patterns share the same phase, however the spatial distortions of the latter correlate with the distortions of the trajectory [8]. With respect to the drive-field sequence  $H_i(t) = H_0 \sin(2\pi f_i t + \phi)$ ,  $i \in \{x, y\}$ , the influence of the drive-field phase  $\phi$  was investigated. Here,  $H_0$  is the drive-field amplitude and  $f_i$  is the drive-field frequency. Utilizing the *MNPDynamics.jl*<sup>1</sup> package and the Fokker-Planck approach, we simulated two system matrices. The first drive field had no phase shift with  $\phi = 0$ , while the second had a phase shift of  $\phi = 0.0783\pi$  (4 samples of 102 samples per period). While both drive fields generate the same trajectories, the latter one starts and ends off-center. Considering a time-shifted periodic signal in frequency domain, the resulting phase shift of the complex frequency signal increases linearly with the frequency index. As shown in Figure 1 b), the resulting system-matrix patterns match in their spatial amplitudes, but their phases increasingly mismatch with increasing frequency index. Installed MPI coil assemblies often do not provide perfectly decoupled drive-field sequences per direction. Von Gladiss et al. showed that remaining coupling of less than 10 % distorts the trajectory significantly [9].

### II.II. Receive signal distortions

Analog to the magnetic field, an inhomogeneous or misaligned receive coil influences the measured signal. In Figure 1 c), the influence of receive coil misalignment with respect to the drive-field direction is shown. Thieben et al. showed that due to the misalignment, the receive channel can not be assigned to one drive-field direction, as signal from multiple directions is induced and as a consequence the system matrix patterns change [7]. In addition, the receive path often includes an analog filter to reduce direct feedthrough from the drive field and a low-noise amplifier to amplify the higher harmonics. These components therefore introduce frequency-dependent distortions in the measured signal [7]. Due to signal processing steps, a time delay between the voltage signal and the digitized signal can occur. Considering a measurement over several frames, this delay leads to same result as the phase shifted drive-field sequence in Figure 1 b).

### II.III. Magnetic field characterization

Magnetic fields inside the FOV fulfill Laplace's equation and thus can be represented by solid harmonic expansions. Boberg et al. showed that instead of sampling the FOV on a grid, by this method, a few measurements on a sphere are sufficient to accurately express the magnetic field inside of this sphere [10].

Using the former method, a 3D Hall probe can be utilized to access inhomogeneities of the static selec-

<sup>1</sup><https://github.com/MagneticParticleImaging/MNPDynamics.jl>

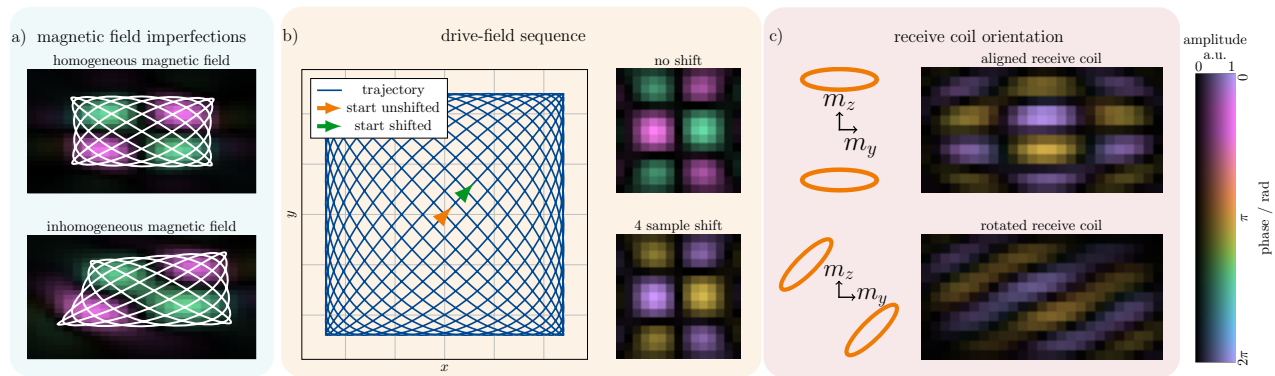


**Figure 1:** Exemplary influence of MPI scanner parameters on the system-matrix patterns. a) Inhomogeneous magnetic fields distort the drive-field trajectory and hence the system-matrix patterns. b) Even small phase shifts of the drive-field sequence lead to increasingly large phase shifts of the system-matrix patterns. c) In the case of misaligned, compared to aligned receive coils (orange) the induced magnetization signal contains portions from multiple drive-field directions.

tion and focus field [10]. For the drive-field sequence, the same method can be applied, but sample-precise knowledge is required. Hence, the measurement must be synchronized with the acquisition signal. For this purpose, Thieben et al. utilized a 3D coil sensor, with defined orientation aligned with the drive-field directions and known turn directions. Thereby, the induced signal by the drive field can directly be connected to the MPI scanner's analog-to-digital converter (ADC) [6]. However, some ADCs include a high-pass filter prior to digitization, that again distorts the measured signal. In this case, only the distortion at the drive-field frequency is of interest. It can be calibrated by an additional measurement with an oscilloscope and a trigger signal. The trigger signal is set to the first sample of the drive-field sequence and triggers the oscilloscope. Hence, for each drive-field direction amplitude and phase of the induced signal are acquired by the oscilloscope. Using Faraday's law of induction with all information of the 3D coil sensor the drive-field sequence can be determined.

#### II.IV. Receive path calibration

The distortions by the receive path of the MPI system can be measured utilizing a 3D calibration coil. Utilizing the coil, Thieben et al. presented a method to determine the MPI transfer function that maps the measured signal to the magnetic moment [7]. To include coil coupling from orthogonal drive-field directions, the MPI transfer function can be measured channel wise and with respect to each direction. The spatial receive coil sensitivity profile can be included, for instance by measuring the MPI transfer function on a sphere with the aforementioned method. Alternatively, the sensitivity profile can be simulated using Biot-Savart law, normalized and multiplied with the MPI transfer function [7]. For send/receive systems (e.g. Bruker MPI 20/25 FF), where the same coils are used for drive-field excitation and signal reception, the

normalized magnetic field profile can be utilized as normalized sensitivity profile due to reciprocity. To assess frequency dependent signal distortions by the ADC an LCR meter can be used to measure the input impedance. The signal processing delay can be identified by utilizing a signal generator that is set to start a sine triggered by the start of the trajectory. The signal generator can then be connected to the ADC and a drive-field sequence can be triggered. From the digitized signal the delay can be measured in units of sample. Here, the delay of the signal generator needs to be taken into account.

#### II.V. Experiment

To validate the presented characterization and calibration methods we utilized the measured system-matrix data and the *particle magnetization model* from Albers et al. [11]. The system matrix was measured on a send/receive system (Bruker MPI 20/25 FF), while the data of the drive-field and sensitivity profile was reused from Thieben et al. [6]. Data of the static selection field was reused from Boberg et al. [10]. Utilizing a 3D coil sensor and an oscilloscope (Siglent SDS 2104X), we analyzed the drive-field sequence by triggering the start of the trajectory. Therefore, the MPI scanner offers a sample precise trigger signal at the start of the trajectory. With respect to the receive path, the MPI transfer function was reused from Albers et al. [11]. We measured the input impedance of the ADC utilizing a vector network analyzer (DG8SAQ VNWA 3) for the frequency range between 10 kHz and 200 kHz. To assess the signal processing delay a signal generator (Rigol DG812) and the oscilloscope was used. The signal generator was set to generate a triggered 200/300 kHz voltage signal with 50 mV amplitude and its delay was measured with the oscilloscope. The signal processing delay after connecting the signal generator to the ADC was measured in units of sample, where 1 sample = 400 ns.

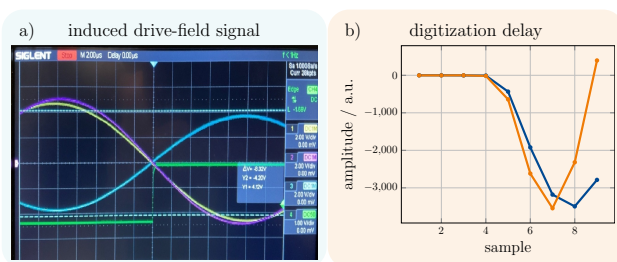


**Figure 2:** Experimental signal analysis. a) Induced drive-field voltage into 3D coil sensor. All drive fields ( $x$ -yellow,  $y$ -violet,  $z$ -blue) have a zero-crossing with the trigger signal (green). b) Digitized signal of the first 9 samples of a drive-field sequence for a 200 kHz (blue) and a 300 kHz (orange) sine are shown. The sine wave is generated by signal generator and is set to start with the start of the drive-field sequence.

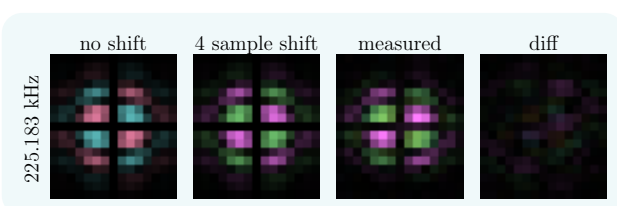


**Figure 3:** Comparison of a modeled and a measured system matrix pattern, with the same 2D complex coded colormap as in Figure 1. From left to right, the modeled system matrix without phase shift, including phase shift, and the measured are shown. On the right, the difference (diff) between the last two is shown.

### III. Results

The input impedance measurement of the ADC resulted in a  $50\ \Omega$  input resistor with a serial capacitor of  $1.5\ \mu\text{F}$ . For the relevant frequencies above 25 kHz the influence of this high-pass filter can be neglected. Figure 2 a) shows the induced drive field signal where all three channels have a zero crossing with the trigger signal within the measurement accuracy. Hence, the drive-field sequence is a cosine sequence. While the  $x$ - and  $y$ -channel do not show an additional phase, the  $z$ -channel has a phase of  $\pi$ . In Figure 2 b) the first 9 samples of the digitized ADC signal are shown. The digitized 200 kHz and 300 kHz sine show a delay of more than 4 samples. Utilizing an oscilloscope a delay of 320 ns ( $< 1$  sample) was measured until the signal generator started to generate the sine wave. Subtracting the 320 ns, the signal processing introduces a delay of more than 3 samples.

Figure 3 shows a system matrix pattern at 225.183 kHz of two MPI transfer function corrected modeled signals, one without and one with a  $\phi = 0.0783\pi$  (4 samples) phase shift, and of a measured signal. Without including the phase shift into the model, major deviations in phase are observed, however the modeled signal with a  $\phi = 0.0783\pi$  phase shift and the measured signal are very

similar and the deviations shown in the difference plot are negligible.

## IV. Discussion and outlook

Detailed a priori knowledge of all parameters of the *MPI scanner model* is required for successful modeling MPI system matrices. In this work, we outlined the effect of scanner parameters on the modeled system matrix and showed that a precise determination of them allows an accurate modeling of the system matrix in phase and amplitude. With a determined *MPI scanner model* at hand, this paves the way to adjusting *particle magnetization model* parameters.

In the future, a more comprehensive examination of the model's sensitivity to each parameter would greatly benefit the calibration process, increasing calibration accuracy while minimizing effort. In addition, with a measured system matrix available, any remaining deviations stemming from uncertainties can be remedied through the use of an MPI transfer-function estimation method [12].

## Author's statement

Authors state no conflict of interest.

## References

- [1] T. Kluth. Mathematical models for magnetic particle imaging. *Inverse Problems*, 34(8):083001, 2018.
- [2] T. Kluth, P. Szwargulski, and T. Knopp. Towards accurate modeling of the multidimensional magnetic particle imaging physics. *New Journal of Physics*, 21(10):103032, 2019, doi:[10.1088/1367-2630/ab4938](https://doi.org/10.1088/1367-2630/ab4938).
- [3] T. Knopp, T. F. Sattel, S. Biederer, J. Rahmer, J. Weizenecker, B. Gleich, J. Borgert, and T. M. Buzug. Model-based reconstruction for magnetic particle imaging. *IEEE Transactions on Medical Imaging*, 29(1):12–18, 2009.
- [4] H. Albers, T. Knopp, M. Möddel, M. Boberg, and T. Kluth. Modeling the magnetization dynamics for large ensembles of immobilized magnetic nanoparticles in multi-dimensional magnetic particle imaging. *Journal of Magnetism and Magnetic Materials*, 543:168534, 2022, doi:<https://doi.org/10.1016/j.jmmm.2021.168534>.
- [5] T. Knopp, H. Albers, M. Grosser, M. Möddel, and T. Kluth. Exploiting the Fourier Neural Operator for faster magnetization model evaluations based on the Fokker-Planck equation. *IJMPI*, 9(1 Suppl 1), 2023, Number: 1 Suppl 1. doi:[10.18416/IJMPI.2023.2303003](https://doi.org/10.18416/IJMPI.2023.2303003).
- [6] F. Thieben, M. Boberg, M. Gräser, and T. Knopp. Efficient 3d drive-field characterization for magnetic particle imaging systems. *IJMPI*, 8(1, Suppl 1), 2022.
- [7] F. Thieben, T. Knopp, M. Boberg, F. Foerger, M. Graeser, and M. Möddel. On the receive path calibration of magnetic particle imaging systems. *IEEE Transactions on Instrumentation and Measurement*, 72:1–15, 2023, doi:[10.1109/TIM.2022.3219461](https://doi.org/10.1109/TIM.2022.3219461).
- [8] M. Boberg, T. Knopp, and M. Möddel. Reducing displacement artifacts by warping system matrices in efficient joint multi-patch magnetic particle imaging. *IJMPI*, 6(2, Suppl 1):1–3, 2020.

- [9] A. von Gladiss, M. Graeser, and T. M. Buzug, Influence of excitation signal coupling on reconstructed images in magnetic particle imaging, in *Informatik aktuell*, A. Maier, T. M. Deserno, H. Handels, K. H. Maier-Hein, C. Palm, and T. Tolxdorff, Eds., event-place: Berlin, Heidelberg, 92–97, Springer Berlin Heidelberg, 2018. doi:[10.1007/978-3-662-56537-7\\_36](https://doi.org/10.1007/978-3-662-56537-7_36).
- [10] M. Boberg, T. Knopp, and M. Möddel. Unique compact representation of magnetic fields using truncated solid harmonic expansions. *arXiv preprint arXiv:2302.07591*, 2023.
- [11] H. Albers, F. Thieben, M. Boberg, K. Scheffler, T. Knopp, and T. Kluth. Model-based Calibration and Image Reconstruction with Immobilized Nanoparticles. *International Journal on Magnetic Particle Imaging IJMPI*, pp. Vol 9 No 1 Suppl 1 (2023), 2023, doi:[10.18416/IJMPI.2023.2303002](https://doi.org/10.18416/IJMPI.2023.2303002).
- [12] M. Boberg, J. Hunecke, F. Thieben, M. Graeser, and T. Knopp. MPI Transfer-Function Estimation with Receive-Coil Coupling. *IJMPI*, 9(1 Suppl 1), 2023, Number: 1 Suppl 1. doi:[10.18416/IJMPI.2023.2303053](https://doi.org/10.18416/IJMPI.2023.2303053).